National Laser Users' Facility News

During FY00 external use of OMEGA increased by 12% and accounted for 50% of the total target shots carried out on the facility. The external users included six teams carrying out work under the National Laser Users' Facility (NLUF) program as well numerous other scientific teams from Lawrence Livermore National Laboratory (LLNL), Los Alamos National Laboratory (LANL), Sandia National Laboratory (SNL), the Nuclear Weapons Effects Testing (NWET) program, and Commissariat à l'Énergie Atomique (CEA) of France.

FY00 NLUF Experiments

The seven NLUF experimental campaigns totaling 124 OMEGA target shots carried out in FY00 included the following:

High-Spatial-Resolution Imaging of Inertial Fusion Target Plasmas Using Bubble Neutron Detectors.
Principal Investigator: Raymond K. Fisher (General Atomics) and collaborators from the University of Rochester (LLE), CEA, and LLNL.

In this experiment, bubble neutron detectors were successfully used for the first time to record neutron images of ICF implosions in OMEGA experiments. The gel bubble detectors were attached to the back of a 10-in. manipulator (TIM) containing a neutron penumbral aperture designed and constructed by a team from the CEA. Figure 84.46(a) shows a photograph of the light transmitted through one of the detectors. Detailed analysis of the bubble density distribution yields the coded image shown in Fig. 84.46(b). The target plane neutron source distribution, obtained from a mathematical inversion of this image, is shown in Fig. 84.46(c). As expected, the counting statistics (resulting from the low neutron detection efficiency of the gel bubble detectors) limit the spatial resolution of this image to ~250 μm. There was no evidence of any background due to x rays or gamma rays. Development of a liquid bubble chamber detector should result in higher neutron detection efficiency and resolution of ~10 to 50 μm.

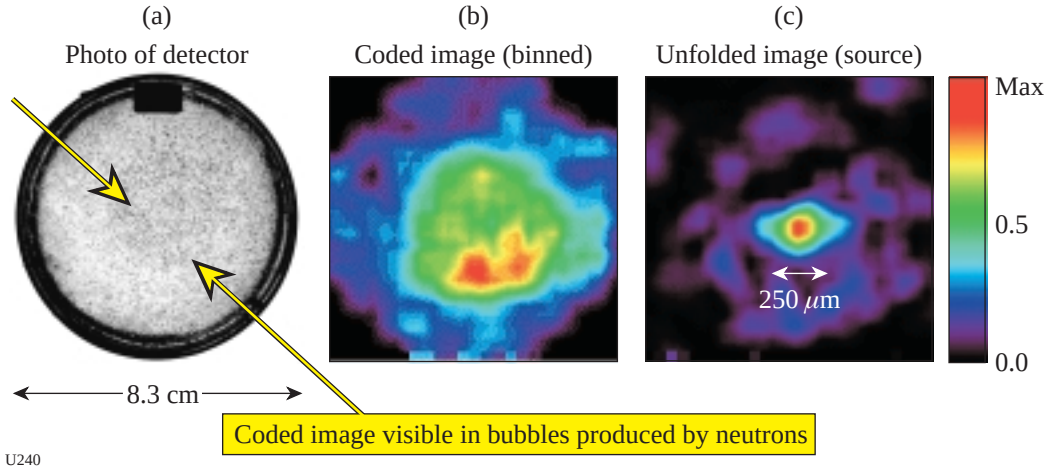

Figure 84.46
(a) Photograph of gel bubble detector after exposure to an OMEGA shot producing 6×10^{13} DT neutrons. The coded image is visible as a circular pattern of bubbles in the center of the detector. (b) Raw digitized coded image. (c) Unfolded neutron image.

Continuing Studies of Dynamic Properties of Shock-Compressed Solids by In-situ *Transient X-Ray Diffraction.* Principal Investigators: Marc Andre Meyers (University of California at San Diego) and Dan Kalantar (LLNL) and collaborators from LLNL, LLE, Oxford University, California Institute of Technology, and LANL.

This work continued a program of studies to investigate the response of crystals to shock compression in regions of strain rates previously unexplored. A series of experiments were conducted to demonstrate the time-dependent compression of a single-crystal Cu sample compressed by direct laser irradiation. Time-resolved streak records of the diffraction from two orthogonal lattice planes in Cu were obtained. Compressions of up to about 3% were observed in both directions at a shock pressure of approximately 200 kbar, confirming that the lattice responds plastically on a nanosecond time scale. A number of different thin-crystal target configurations were tested to identify and resolve issues of x-ray preheat due to the laser drive, and a mixed backlighter was tested to measure the compression of different parallel lattice planes. In addition, simultaneous shock compression and post-shock recovery experiments were conducted with single-crystal Cu to relate the residual damage to the *in-situ* diffraction measurements (Fig. 84.47). A series of nine 1-mm-thick Cu samples were shocked and recovered for post-shot TEM analysis.

Supernova Hydrodynamics on the OMEGA Laser. Principal Investigators: Paul Drake (University of Michigan) and Bruce Remington and Harry Robey (LLNL) and collaborators from LLNL, LLE, CEA, Osaka University, University of Arizona, University of Chicago, Eastern Michigan University, State University of New York–Stony Brook, and West Point Military Academy.

Supernovae are not well understood. Recent observations have clarified the depth of our ignorance by producing observed phenomena that current theory and computer simulations cannot reproduce. Such theories and simulations involve, however, a number of physical mechanisms that have never been studied in isolation. In this project, which this year involved 22 co-investigators from 11 institutions, well-scaled

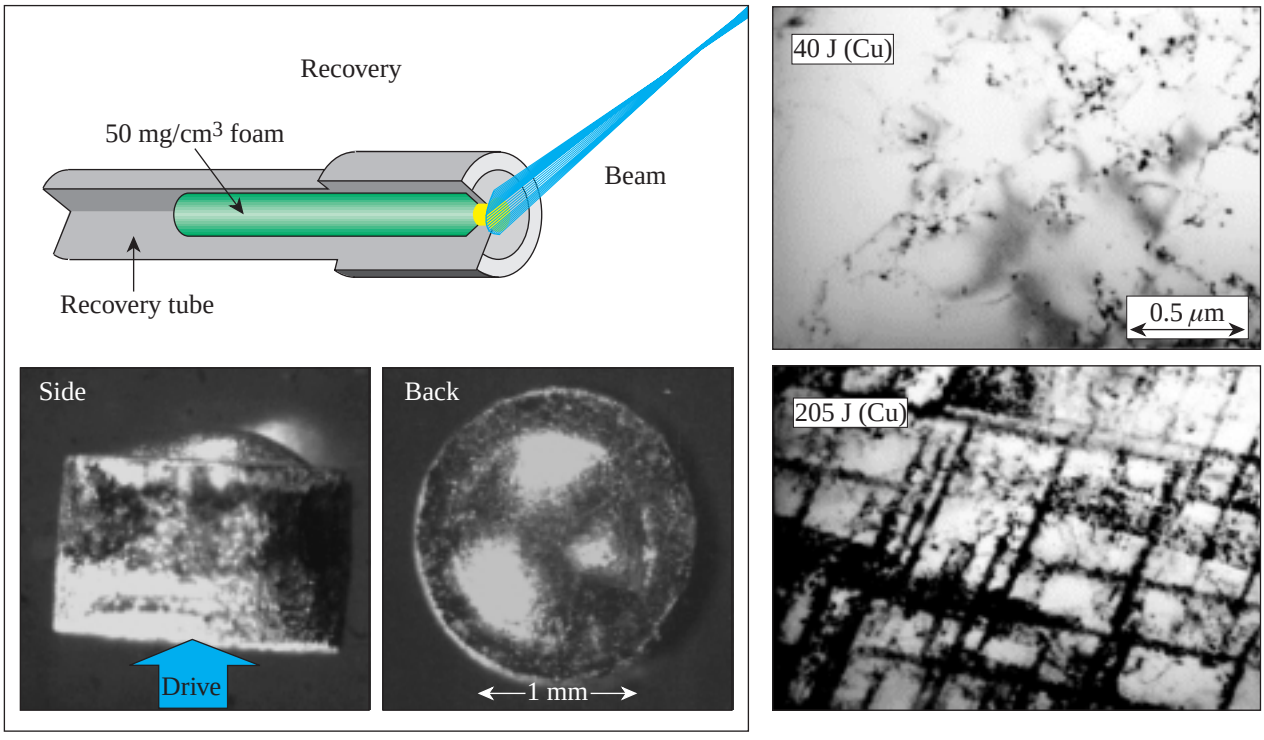

Figure 84.47
Illustration of crystal recovery experiments. Top left: the experimental configuration. Bottom left: photographs of a recovered Cu sample. Right: post-shot TEM photographs of shocked Cu samples shocked with a 40-J laser pulse (top) and a 205-J laser pulse (bottom). These samples were compressed at extreme strain rates, but they show similar residual dislocation and other microstructure as crystals shocked in lower-strain-rate gas-gun experiments.

experiments conducted on OMEGA investigated such mechanisms. Such experiments also provide clear tests of the codes used to simulate astrophysical phenomena. This past year's experiments were also used to observe interface coupling. In this case a shock wave was perturbed by structure at a Cu/plastic interface, and it in turn caused structure to evolve at a plastic/foam interface. Experiments were also conducted to study hydrodynamic instability growth at a spherically diverging interface (see Fig. 84.48). In addition, experiments were initiated to compare instability growth in 3-D versus 2-D, to examine the growth of multimode perturbations, and to produce and diagnose a radiative precursor shock.

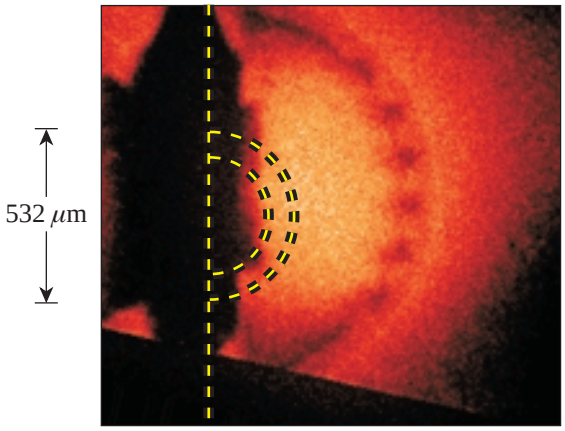

Figure 84.48
X-ray radiograph showing modulations on a spherical capsule that has expanded into resorcinol foam of density ~100 mg/cm^3. The initial outside diameter of the Br-doped CH capsule was 532 μm and the wall thickness was 97 μm. Initial perturbation wavelength and amplitude were 70 μm and 10 μm, respectively. Hydrodynamic instabilities, like those present in supernovae, caused the observed modulations to develop from the small initial perturbations.

Charged-Particle Spectroscopy on OMEGA: Recent Results, Next Steps.
Principal Investigator: Richard Petrasso (Massachusetts Institute of Technology) and collaborators from LLNL, LLE, and SUNY Geneseo.

The focus of this year's work has been the acquisition and interpretation of high-resolution secondary proton spectra [Fig. 84.49; see also LLE Review **83**, 130 (2000)]. These results are important not only for the information obtained for the current gas-filled capsule implosion experiments but also in demonstrating the potential to characterize cryogenic-target implosions. Secondary-proton spectroscopy may provide one of the best means for studying high-density cryogenic capsule implosions.

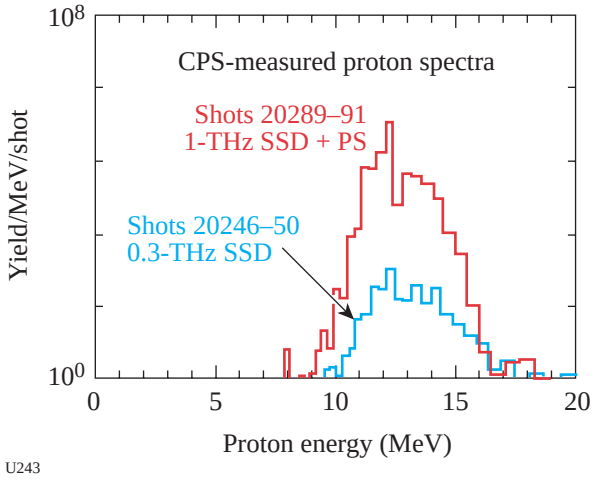

Figure 84.49
Comparison of multishot-averaged secondary proton spectra obtained with the CPS 2. Shots 20289 to 20291 were carried out with improved uniformity (1-THz, 2-D SSD and polarization smoothing), while shots 20246 to 20250 were carried out with 0.3-THz, 2-D SSD and no polarization smoothing. Note the higher secondary proton yields and increased energy downshift (indicating higher shell areal density) for the improved uniformity implosions.

Development of X-Ray Tracer Diagnostics for Radiatively Driven NIF Ignition Capsule Ablators.
Principal Investigator: David Cohen (Prism Computational Sciences) and collaborators from the University of Wisconsin, LLE, LANL, SNL, and LLNL.

This program continued a series of x-ray spectroscopic measurements to explore the physics of radiation-driven, NIF-type ablators. The FY00 campaign included two days of shots in which time-dependent backlit absorption spectra were measured from thin tracer layers buried inside capsule ablator samples that were mounted on halfraums (see Fig. 84.50). A significant signal was observed from NaCl tracers (Cl K_α) in both germanium-doped and undoped plastic ablator samples. The onset of the signal was seen to be delayed in the doped sample as compared to the undoped sample. Furthermore, especially in the doped sample, the progressive heating of the tracer can be seen as the dominant ionization state moves from Be-like to He-like over an interval of ~100 ps (Fig. 84.51). These data demonstrate the effects of ablator dopants on the radiation wave characteristics. Among other innovations in this year's campaign, we were able to construct targets and mount diagnostics in such a way as to do simultaneous spectroscopy of two samples on a single halfraum using two

different time-resolved spectrometers. These experiments are relevant for ablator characterization and target design efforts for NIF ICF targets.

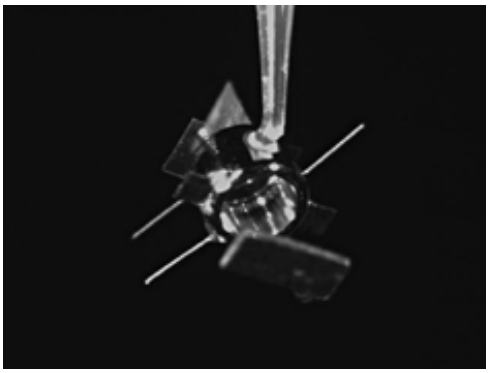

U244

Figure 84.50
A Powell-scope image of a halfraum target, seen from the laser entrance hole (LEH) side. The rectangular object in front of the LEH is a bismuth backlighter foil. The positioning stalk can be seen at the top of the barrel of the halfraum, and various positioning fibers and shields are also visible. The ablator sample (in the form of a witness plate) is on the back end of the cylinder.

Investigation of Solid-State Detection of Charged-Particle Spectrometry.
Principal Investigator: Kurtis Fletcher (State University of New York at Geneseo) and collaborators from MIT, LLE, and LLNL.

In this collaboration, electronic detection of charged particles was demonstrated using the charged-particle spectrometer (CPS1) on OMEGA. A 250-μm-thick pin diode was mounted in the spectrometer focal plane at the position corresponding to ~15-MeV protons. In a series of shots with D^3He-filled CH shells, high-energy protons passed through a collimator, an Al filter, and a CR-39 track detector before stopping in the diode. Each proton deposited about 3.5 MeV of energy in the diode. The resulting voltage signal of the diode was recorded on an oscilloscope [see Fig. 84.52(a)]. The CR-39 detector for each shot was later etched and the number of protons counted to provide a benchmark for the electronic detection system. As expected, the area of the proton peaks was proportional to the number of protons [see Fig. 84.52(b)]. This project demonstrated proof-of-principle that electronic detection of charged particles generated in the ICF environment is possible under appropriate conditions.

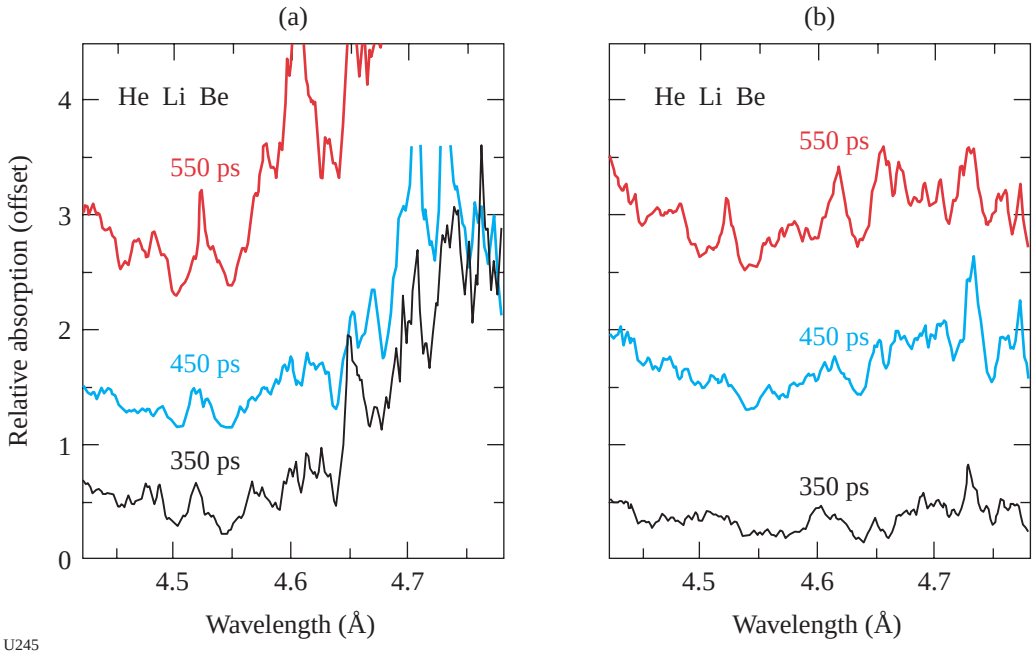

U245

Figure 84.51
Time-resolved absorption spectra of chlorine features from (a) an undoped sample and (b) a doped sample. The three prominent tracer absorption features are marked on each figure. The three lineouts shown in each figure are time-averaged over 100 ps.

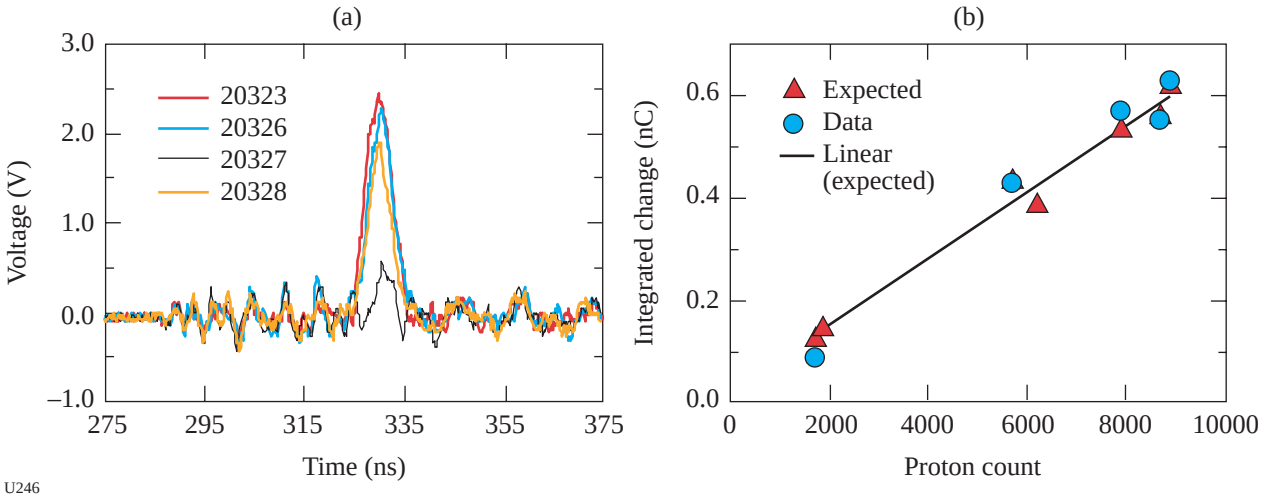

Figure 84.52
(a) Solid-state (PIN)-detector primary proton signals obtained on four shots (20323, 20326, 20327, and 20328) on D^3He-filled CH shells. (b) Integrated charge on solid-state detector versus the proton count as measured with a CR-39 track placed ahead of detector.

Optical Mixing of Controlled Stimulated Scattering Instabilities (OMC SSI) on OMEGA II.
Principal Investigator: Bedros Afeyan (Polymath Research Inc.) and collaborators from LLNL, LANL, and LLE.

In this collaboration, experiments continued to investigate optical-mixing-controlled stimulated scattering instabilities in NIF-like, long-scale-length plasmas. This year, the OMC SSI experiments concentrated on extending the previous results showing stimulated Raman scattering (SRS) backscattering reduction of an interaction or pump beam in the presence of an overlapping (probe) laser beam at the Mach = –1 surface. The interaction of the two beams is expected to produce a spatially localized, large-amplitude ion-acoustic wave (IAW). This IAW in turn dephases the SRS instability by producing IAW turbulence. The dependence of the nonlinear interaction processes on pump and probe beam intensity, probe beam spot size, and crossing region location were investigated in the FY00 experiments. Some of the results of these experiments are shown in Fig. 84.53.

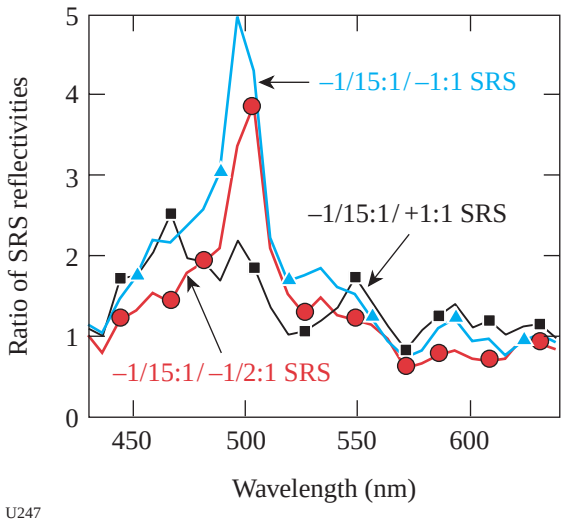

Figure 84.53
Ratio of stimulated Raman backscattering (SRBS) reflectivities plotted versus wavelength integrated over time. The plot shows weak-probe SRBS reflectivities where the intensity ratio between probe and pump beams is 15:1, divided by strong-probe SRBS reflectivities where the intensity ratio between probe and pump is 1:1 (blue curve) and 1/2:1 (red curve) and the probe beam is focused where the flow velocity is Mach = –1. The black curve is the control; the intensity ratio of pump to probe is 1:1 but the beams are focused where the flow is Mach = +1, where no resonant ion wave can be driven by the interaction of pump and probe. The black curve is not flat at M = +1 because even at that focus some of the light does get to Mach = –1, giving a slight reduction of the SRBS.

FY01 NLUF Proposals

A record 17 proposals with funding requests totaling $3,685,742 (total for FY01 and FY02) and with shot requests of 360 and 370 shots, respectively, in FY01 and FY02 were submitted to NLUF this year. For the first time, the successful proposals will be approved for a two-year period of performance (FY01 and FY02).

A DOE technical evaluation panel including Dr. David Bradley (LLNL), Dr. David Montgomery (LANL), Dr. Richard Olson (SNL), and Dr. Ned Sautoff (Princeton Plasma Physics Laboratory) reviewed the proposals on 19 May 2000. The NLUF Manager (non-voting) chaired the panel. The committee recommended approval of eight of the proposals (see Table 84.VII) with reduced funding and shot allocation to fit within the budget of $700,000 per year and NLUF shot allocation of 120 shots per year. A ninth proposal was conditionally approved pending additional funds from DOE.

FY00 National Laboratory, NWET, and CEA Programs

When Nova operations ended in FY99, national laboratory and other use of OMEGA continued to increase. Programs of the three national laboratories (LLNL, LANL, and SNL), NWET, and CEA accounted for over 38% of OMEGA use during this fiscal year. The following is a brief summary of some of the work carried out by the national laboratories, NWET, and CEA:

1. LLNL and NWET Campaigns

In FY00 LLNL had 320 shot opportunities at the OMEGA facility, divided as follows: 100 shots for target ignition physics (TIP), 200 shots for high-energy-density science (HEDS), and 20 shots for nuclear weapons effects testing (NWET). A total of 284 target shots were taken. These shots involved 15 Principal Investigators (including shots with collaborators from SNL and LANL) and spanned the 21 different mini-campaigns listed in Table 84.VIII.

Highlights of LLNL experiments include the following:

Conversion Efficiency: An initial OMEGA campaign was carried out to investigate the x-ray drive energetics in roughened hohlraums. Roughened hohlraums are required for infrared augmented β-layering on NIF, and the initial OMEGA results indicate that the rough hohlraums appear brighter than the smooth ones, contrary to expectations.

Cocktail Hohlraums: Experiments were initiated on OMEGA to investigate the soft x-ray emission of "cocktail" materials—i.e., mixtures of elements rather than the conventional Au-lined hohlraum. The initial results are in agreement with *LASNEX* simulations, and experiments will continue to confirm the expectations of higher drive with cocktail materials.

NIF Foot Symmetry: NIF-scale, 90-eV hohlraum symmetry experiments were carried out on OMEGA with a novel point-projection backlighting technique to assess the symmetry of drive in the foot of the NIF pulse. The results of these experiments indicate that the technique is capable of 1% accuracy in detecting asymmetry modes in NIF-scale targets.

Table 84.VII: Approved NLUF Proposals for FY01/02

Principal Investigator	Affiliation	Title of Proposal
C. F. Hooper, Jr.	University of Florida	Atomic Physics of Hot, Ultradense Plasmas
R. Mancini	University of Nevada, Reno	Determination of Temperature and Density Gradients in Imploded Cores of OMEGA Targets
R. Petrasso	Massachusetts Institute of Technology	Studies of Fundamental Properties of High-Energy-Density Plasmas
H. Baldis	University of California - Davis	Studies of Dynamic Properties of Shock-Compressed FCC Crystals
R. K. Fisher	General Atomics	High-Spatial-Resolution Neutron Imaging of Inertial Fusion Target Plasmas Using Bubble Neutron Detectors
R. B. Stephens	General Atomics	Asymmetric Fast Ignition Target Compression
P. Drake	University of Michigan	Supernova Hydrodynamics on the OMEGA Laser
B. B. Afeyan	Polymath Research, Inc.	Optical-Mixing-Controlled Stimulated Scattering Instability Experiments on OMEGA III and IV: Suppressing Backscattering Instabilities by the Externally Controlled Generation of Ion Acoustic Wave or Electron Plasma Wave Turbulence

High-Convergence Implosions: The multicone capability of OMEGA was used to conduct hohlraum-driven implosion experiments with an inferred convergence ratio up to 20. The resulting neutron yield on these implosions was significantly improved compared to the previous Nova results with a single cone of beams (see Fig. 84.54).

Shock Timing: Using a shock optical pyrometer (SOP), the UV emission of shock breakout was measured and used to infer shock velocity in radiation-driven ablators. Shock propagation data were obtained for Al, polyimide, and Be+0.9% Cu samples. These experiments were carried out in a collaboration involving SNL, LANL, LLNL, and UR/LLE.

Ablator Burnthrough: SNL led a team of LLNL, LANL, and LLE scientists in conducting an experiment to investigate burnthrough in a radiation-driven capsule. The experiment was designed to provide verification of ICF ablator burnthrough timing. Indirect-drive burnthrough data were obtained for polyimide and beryllium samples using the half-hohlraum (halfraum) geometry shown in Fig. 84.55(a). Spatially resolved streak camera imaging was used in conjunction with timing fiducials provided by two of OMEGA's beams to provide this data [see Fig. 84.55(b)].

Convergent Ablator Burnthrough: X-ray-backlit implosions were used to determine the ablation rate and payload trajectory in spherical geometry in the hohlraum drive. Some of the results from these experiments are shown in Fig. 84.56.

Planar RT: Polyimide ablator Rayleigh–Taylor growth measurements were conducted on radiation-driven planar targets on OMEGA. The initial OMEGA experiments show acceptable agreement with code predictions for all wavelengths (see Fig. 84.57).

Table 84.VIII: LLNL Campaigns on OMEGA in FY00.

Campaign	Sub-Element	Experiment	Target Shot Allocation
Target Ignition Physics	WBS 1 – Energetics	Conversion efficiency	15
		Laser–plasma interaction	10
		Cocktail hohlraums	5
	WBS 2 – Symmetry	NIF foot symmetry	20
		High-convergence implosions	5
	WBS 3 – Ablator Physics	Shock timing	15
		Ablator burnthrough	10
		Convergent ablator burnthrough	10
		Planar RT	10
High-Energy-Density Sciences	Solid-State Hydro		15
	Implosion Mix	Pushered shells	15
	Hydro I	Richtmyer–Meshkov	40
	Hydro II	Features	20
	Hydro III	Jets	20
	Radiation Transport	Low T_r drive	5
		Radiation transport in foams	30
	Equation of State (EOS)	Low- and high-Z EOS	35
	Capability Development	Backlighter development	15
		Fluorescence mix	5
Nuclear Weapons Effects Testing (NWET)	Source Development	Gas-filled-Be-can sources	10
		Hot-electron sources	10

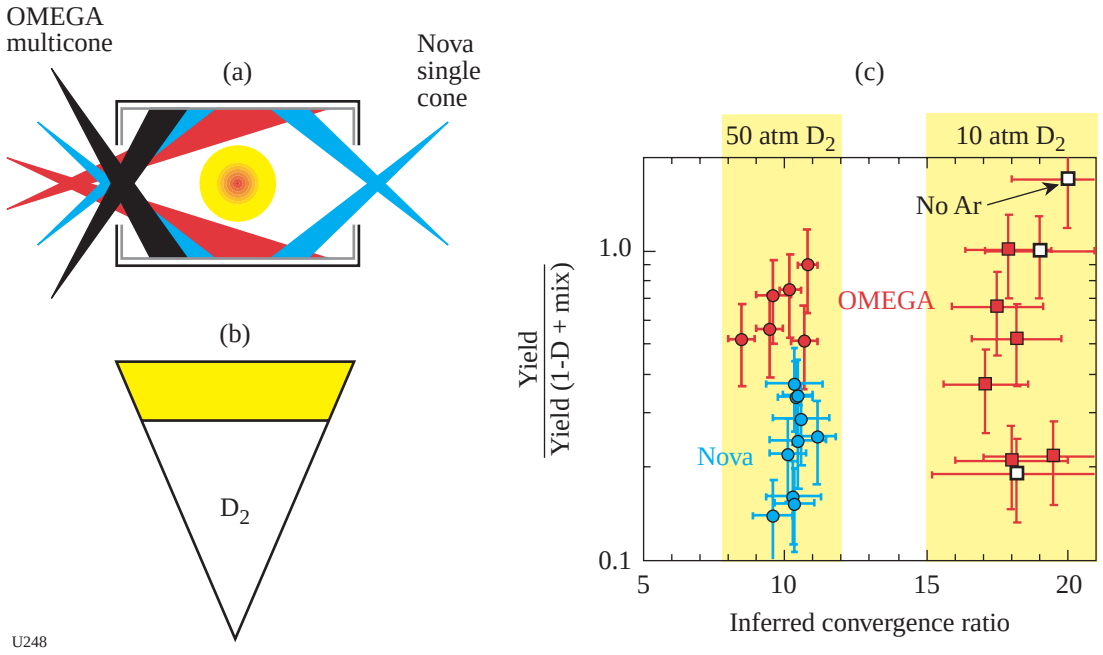

Figure 84.54
(a) Schematic illustrating the beam configuration for OMEGA compared to Nova. (b) Typical capsules used in these experiments were D_2-filled, Ge-doped CH shells. (c) Plot of the ratio of the measured neutron yield over the calculated 1-D yield including mix as a function of the inferred convergence ratio. The low-convergence-ratio targets contained 50 atm of deuterium (data points are circles), while the higher-convergence-ratio targets contained 10 atm (square data points). The open data points contained no Ar doping in the fuel. The Nova points are blue and the OMEGA data are red.

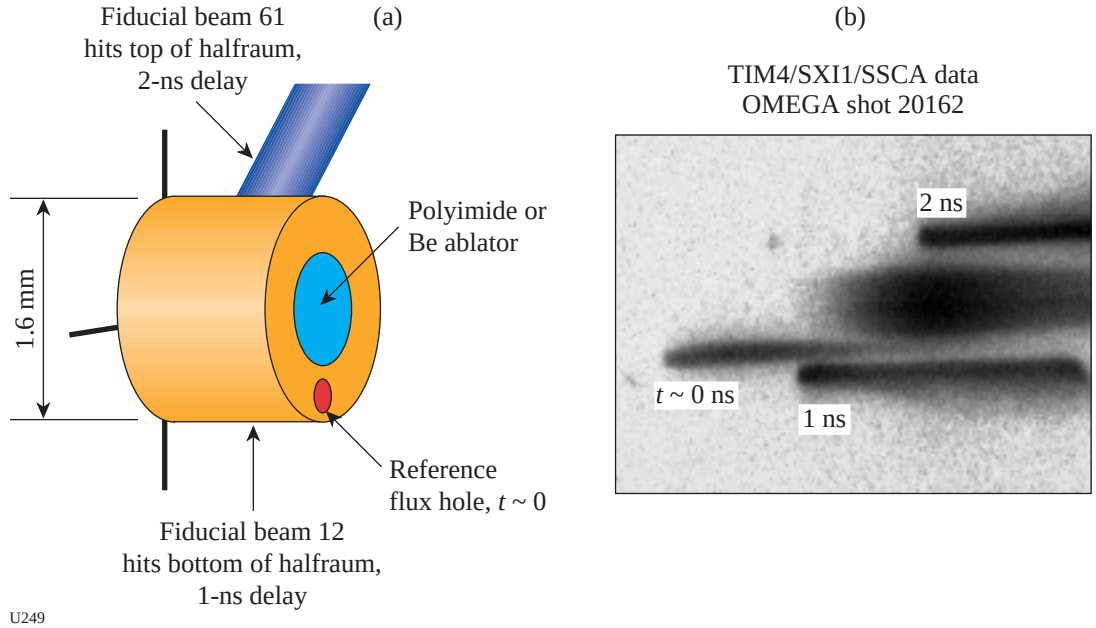

Figure 84.55
(a) Schematic of burnthrough experiment. Fifteen drive beams are brought into the halfraum in two cones, while two beams irradiate the top and bottom of the exterior of the halfraum to provide timing fiducials. A hole in the halfraum provides a time history of the x-ray flux in the halfraum. (b) Streak camera record of x-ray emission showing the reference flux hole emission ($t \sim 0$) and delays ($t \sim 1$ and 2 ns) along with the central delayed feature signaling burnthrough to the ablator being used in this experiment.

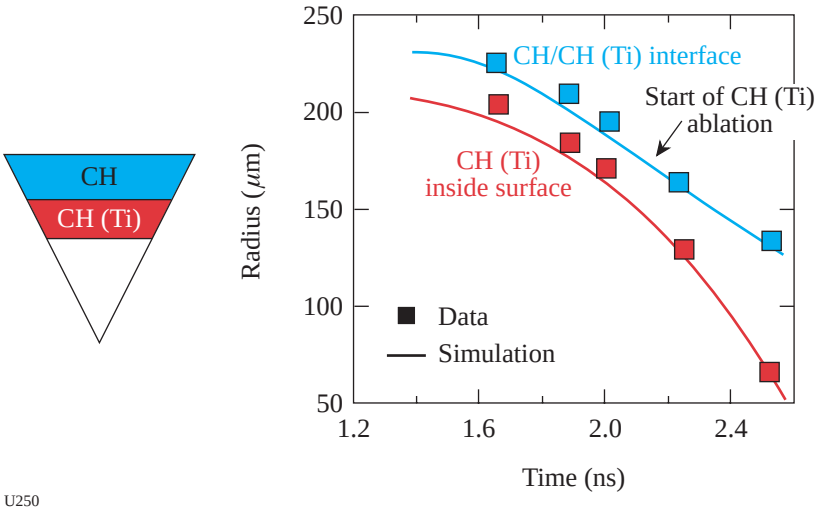

Figure 84.56
Measurement of ablation rate and payload trajectory in a hohlraum-driven spherical implosion experiment. The ablator for this experiment was CH, and an inner layer of Ti-doped CH served as the signature of ablator burn-through. Time-gated radiography with 5.2-keV x rays was used to make this measurement.

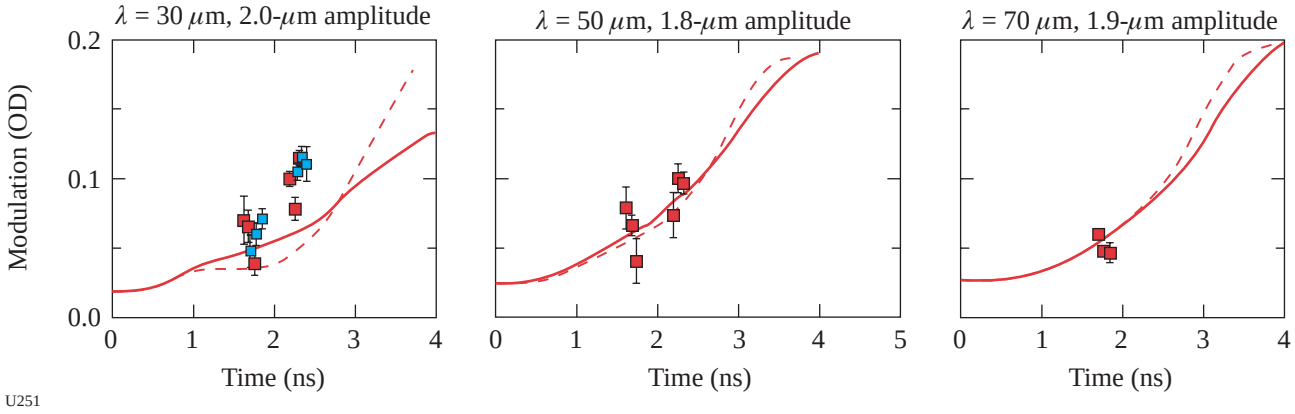

Figure 84.57
Results of Rayleigh–Taylor growth measurements on radiation-driven polyimide foils. These three plots show the measured modulation (OD) as a function of time for three radiation-driven planar targets with different initial wavelengths and amplitudes. The dashed lines represent simulations using a Planckian spectrum, while the solid lines represent the simulations using Dante-derived drive and calculated spectrum.

Pushered Shells: Experiments were conducted on a hohlraum-driven, single-shell target design consisting of a DT-filled glass shell overcoated with Ge-doped CH. The neutron burn history, neutron yield (20% of clean yield), radiation drive, and absorption imaging of the CH/SiO_2 trajectory were compared to hydrodynamics simulations.

Hydrodynamics: Several important hydrodynamics campaigns were carried out on OMEGA in FY00. A new shock-driven hydrodynamics geometry was successfully tested, and VISAR measurements of shock velocity were carried out. Simultaneous side-on and face-on data were obtained and 3-D features clearly observed on the interaction of a shock and a sphere. A collaborative experiment between the AWE (United Kingdom), LANL, and LLNL investigated the interaction of a supersonic jet with a counter-propagating shock. These experiments were simulated using the *RAGE* code at LANL, the *CALE* code at LLNL, and the *NYM-PETRA* code at AWE.

Long, Low T_r Drive: X-ray diffraction was used to measure melt and 1-D to 3-D lattice transitions on OMEGA. Simultaneous measurements of Bragg and Laue patterns on Cu showed 3-D compression of the crystal lattice.

Radiation Transport in Foams: The importance of wall structure and wall losses was demonstrated in experiments on foam-filled hohlraums.

Low- and High-Z EOS: Equation of state of relevant materials was measured at high pressures (1 to 50 Mbar) on OMEGA.

These experiments were conducted in both direct- and indirect-drive mode and showed that preheat is an issue for both approaches for these measurements.

Backlighter Development: A new backlighting capability was validated that will be used on NIF hydro experiments. This technique is pinhole-assisted point projection backlighting. Ultrahigh (100×)-magnification x-ray imaging was carried out to measure the core of OMEGA hohlraum-driven target implosions. This approach has the capability of providing 3-μm resolution at an x-ray energy of 6 keV.

Gas-Filled-Be-Can X-Ray Sources: Experiments were carried out on OMEGA to investigate the x-ray production of internally irradiated gas- and foam-filled Be cans. High conversion efficiency (~10%) to Ar *K*-shell and Xe *L*-shell radiation was measured for Ar- and Xe-filled Be cans. Foam-filled (6 mg/cm^2 SiO_2) cans demonstrated 30× enhancement of 50-keV x rays compared to previous measurements with 1% of critical density (n_c) C_6H_{12} gas-filled cans.

2. LANL Campaigns

Los Alamos National Laboratory conducted several experimental campaigns at OMEGA during FY00 as part of Campaign 10 Major Technical Efforts in Indirect-Drive Ignition and Support for Stockpile Stewardship. These campaigns included the following:

Double Shells: These experiments showed that the performance of the reduced M-band absorption (imaging) double-shell target exceeds that of all others at convergence ratio (CR) ~38 (see Fig. 84.58).

Classified Experiments: Classified experiments with important results were successfully hosted by LLE.

Direct-Drive Cylinder Experiments (DDCYL): DDCYLMIX experiments achieved good "low-mix/high-mix" comparison with well-characterized conditions for compressible plasmas in convergent geometry (see Fig. 84.59). Static targets better characterized the details of image analysis and careful comparison to theoretically simulated radiographs.

Backlighter Studies: Energy and intensity-dependent scaling for *K*-shell backlighters were determined for NIF-relevant backlighters. A series of experiments (Fig. 84.60) were carried out using Fe, Zn, and Ge backlighter targets driven at relatively high laser intensity (1×10^{16} W/cm^2).

High-Convergence Implosions: X-ray imaging of single-shell implosions showed transition from a limb-brightened image to a centrally peaked image at CR~23, indicative of mix.

Spike Dissipation: Laser-based experiments have shown that Rayleigh–Taylor growth in thin, perturbed copper foils leads to a phase dominated by narrow spikes between thin bubbles. These experiments are well modeled and measured until this "spike" phase, but not into the spike phase. Experiments were designed and carried out on OMEGA to explore the late-time spike phase. The OMEGA experiment used side-on radiography with a 6.7-keV Fe backlighter source. A gated x-ray imager time-resolved the x-ray transmission image from which the temporal development could be obtained (Fig. 84.61).

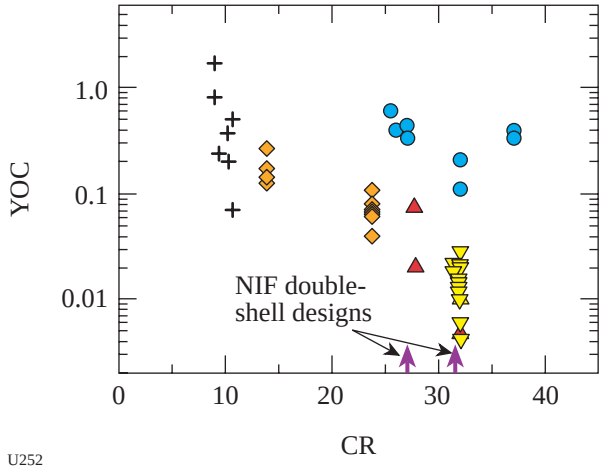

Figure 84.58
Ratio of measured neutron yield over the calculated clean yield (YOC) plotted as a function of calculated convergence ratio for indirect-drive Nova and OMEGA experiments. The diamonds indicate Nova cylindrical-hohlraum single-shell shots (1.4-ns square pulse shots). The crosses are data from tetrahedral-hohlraum single-shell-capsule experiments on OMEGA (1-ns square pulse). The inverted triangles represent standard double-shell data taken on OMEGA. The upright triangles represent suppressed M-band hohlraum double-shell-target data, and the solid circles represent reduced M-band absorption double-shell-capsule data taken on OMEGA. The arrows indicate NIF double-shell ignition designs with foams of 0.15 g/cc and 0.1 g/cc at convergence ratios 24 and 33, respectively.

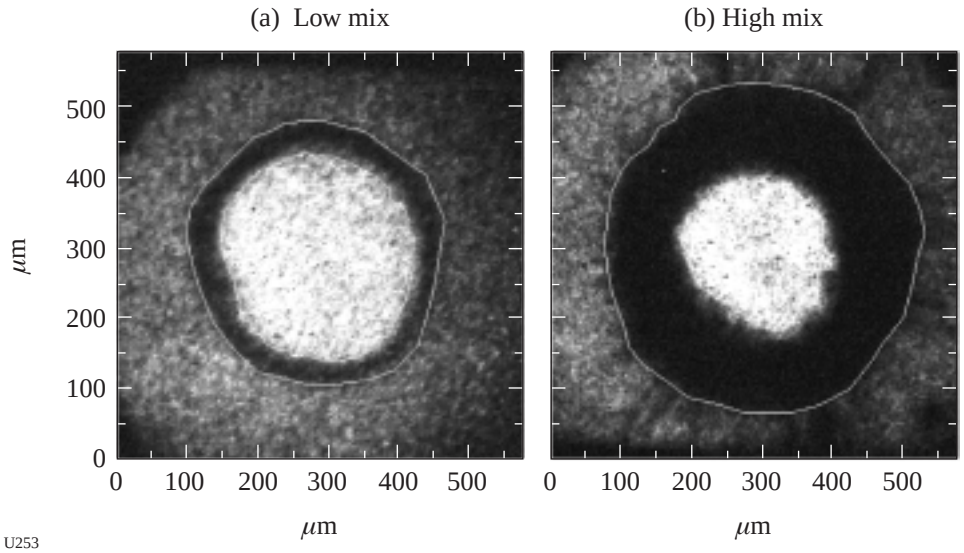

U253

Figure 84.59
X-ray radiographs taken along the cylinder axis of directly driven cylindrical target implosions. (a) Shot 18689 (19.1 kJ with Fe backlighter) low-mix target with dichloroprolystyrene marker layer (initial Atwood number = 0.15); (b) (Shot 18687 (19.9 kJ with Ti backlighter) high-mix target with Au marker layer (initial Atwood number = 0.95). Both images are taken 4.75 ns after t_0 in mass-matched implosions.

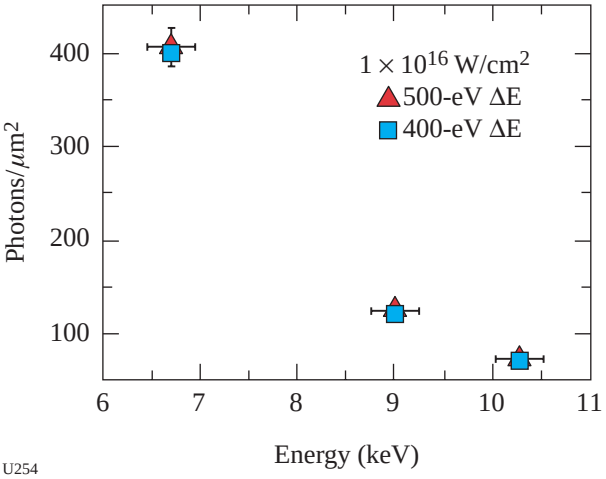

U254

Figure 84.60
X-ray fluence in photons per square micron plotted as a function of x-ray energy for Fe (6.7 keV), Zn (9.0 keV), and Ge (10.3 keV) *K*-shell x-ray emitters. The triangles represent 500-eV energy bandwidth, and squares represent 400-eV bandwidth. The experiments were carried out at an on-target intensity of 10^{16} W/cm^2.

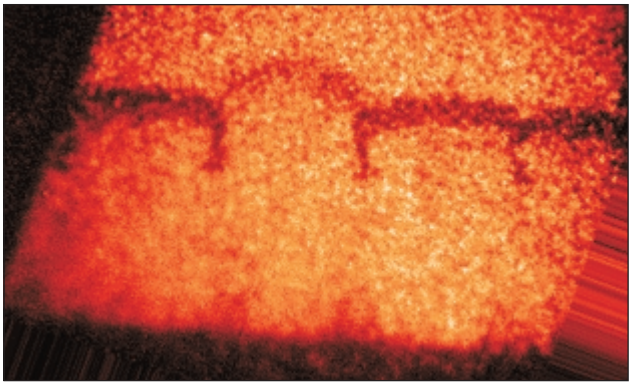

U255

Figure 84.61
Typical radiograph obtained on spike evolution experiment. The Cu target in this case was milled to generate a series of 10- to 20-μm-thin, 200-μm-long, 30-μm-high ridges 150 μm apart, leaving a thin, flat Cu backing. The target was placed on the side of a scale-1.2 OMEGA hohlraum with the ridges pointing into the hohlraum. A laser drive consisting of 1-ns square pulses heated the hohlraum to 190 eV to drive the target. The image shows the growth of the spikes and mushroom-like feet on the tips of the spikes.

High-Yield Neutron Shots for Diagnostic Development: NIF Phase 2 (Advanced) neutron diagnostics for burn history and neutron imaging were fielded, with first observations made of fusion gammas from an ICF target. The signal shown in Fig. 84.62 is from a Gas Cerenkov burn history diagnostic implemented on OMEGA.

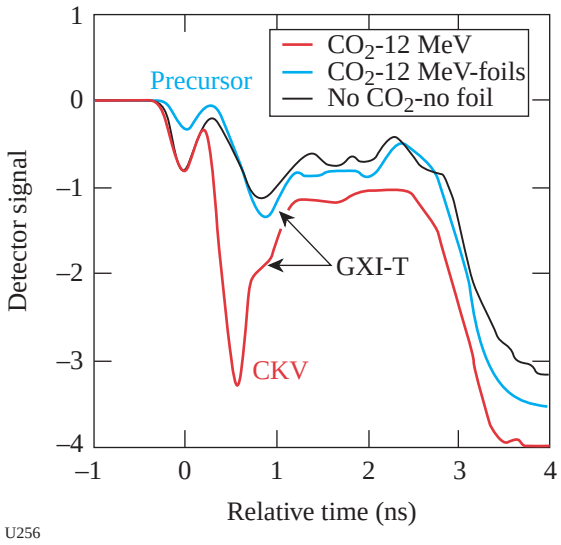

Figure 84.62
Typical Gas Cerenkov counter detector response for a high-neutron-yield, DT-filled-capsule shot (red line). The Cerenkov signal is the peak at ~0.6 ns (marked CKV). The plot also shows the signals from two other shots where the Cerenkov signal was blocked (black line) and where there was no CO_2 gas in the counter (blue line). The small hump in the back of the Cerenkov signal is apparently due to gamma rays generated by interaction of the neutrons generated in the implosion and the GXI diagnostic.

Los Alamos also supported several other campaigns at OMEGA:

Sandia WBS 3 ablator characterization, NLUF laser–plasma instability work, AWE Jet experiment, and transient x-ray diffraction materials work.

3. CEA Activities

In FY00, CEA (France) activities on OMEGA included the installation and activation of two diagnostics—a penumbral neutron imaging system (NIS) and an absolutely calibrated time-resolved broadband x-ray spectrometer (DMX)—and x-ray conversion efficiency experiments in spherical geometry.

Time-Resolved Broadband X-Ray Spectrometer (DMX): DMX (see Fig. 84.63) is a broad-bandwidth, absolutely calibrated x-ray spectrometer that uses new coaxial x-ray detectors (CXRD) to provide an overall ~100-ps temporal resolution in a compact 20-channel instrument. Spectral resolution is obtained by a combination of mirrors, filters, and detector spectral response. The current configuration covers a range of 50 eV to 20,000 eV. DMX was successfully activated and compared with a similar instrument (LLNL's Dante) on OMEGA shots in both direct and indirect drive. A satisfactory agreement was found between the two diagnostics on spectral shape and x-ray emission time history under various conditions (Fig 84.64), but a discrepancy was observed on absolute levels between the two diagnostics.[1] Further work is in progress to understand the origin of this discrepancy.

X-Ray Conversion Experiments: X-ray conversion experiments on disks are sensitive to 2-D effects. The OMEGA configuration delivers a very uniform laser irradiation pattern, enabling a quasi 1-D experiment in spherical geometry very suitable for the validation of numerical simulations. A set of experiments were carried out to study x-ray conversion on gold-coated, 950-μm-diam CH spheres (2.5 to 3 μm gold thickness) at laser intensities ranging from 3×10^{13} up to 8×10^{14} W/cm^{-2}. X-ray conversion history at different energies, x-ray imaging of plasma, and spectral measurements were used as benchmark simulations.

Neutron Imaging of an Imploding DT Target: Recently, CEA installed a new 14-MeV neutron imaging system (NIS) on OMEGA. This diagnostic measures the size of the neutron-emission area of a direct-drive implosion. A neutron image resolution better than 10 μm is required on future laser facilities such as LMJ and NIF. In June a prototype NIS was tested on OMEGA, using the technique of penumbral imaging, which has an ultimate resolution of 30 μm. The aperture is a massive cylinder (50 mm thick) of tungsten alloy, inside which an aperture with a biconical shape is drilled. The shape of this aperture is defined by entrance, middle, and output diameters of 600 μm, 760 μm, and 1070 μm, respectively. The entrance side of the aperture is set at 55 mm from the target with an aperture manipulator installed into a TIM. The aperture is positioned by a four-stage piezoelectric vacuum compatible actuator, which was tested in a high neutron flux environment. The image is recorded on a detector installed on the Target Bay floor at 8 m from the target chamber center (TCC). The detector is composed of 8000 plastic scintillating fibers. The light is generated mainly by the slowing of a proton produced by elastic scattering of a neutron on hydrogen. The resulting optical image is then amplified by a gated microchannel plate and recorded on the CCD. The CCD is protected from the direct interaction of the neutron by a shield made with polyethylene

and lead. The coded image [see Fig. 84.65(a)] is then unfolded by a filtered autocorrelation technique to produce the image shown in Fig. 84.65(b). The source is observed to be 120 μm in diameter on this shot and can be compared with the 3-keV x-ray image obtained on the same shot.

REFERENCES

1. See J. L. Bourgade *et al.*, "DMX: An Absolutely Calibrated Time-Resolved Broadband Soft X-Ray Spectrometer Designed for MJ Class Laser-Produced Plasmas," to be published in the Review of Scientific Instruments.

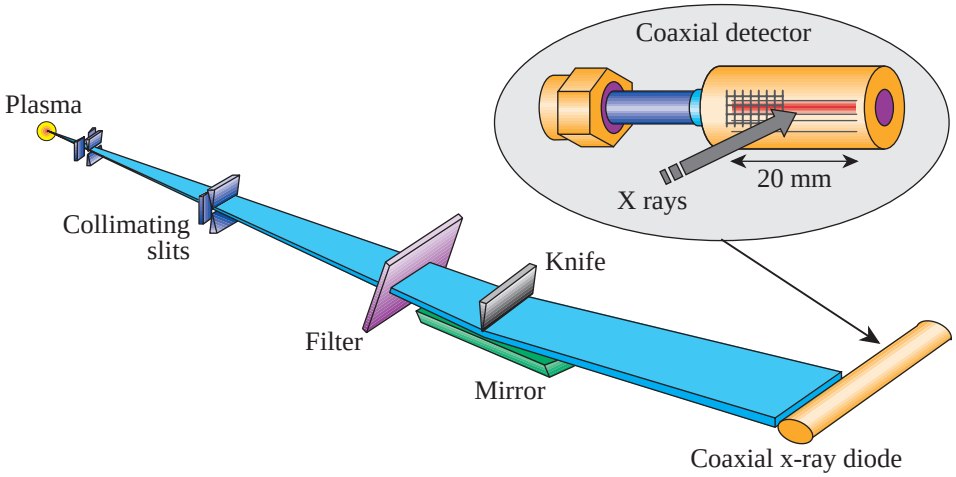

Figure 84.63
Illustration of a DMX diagnostic.

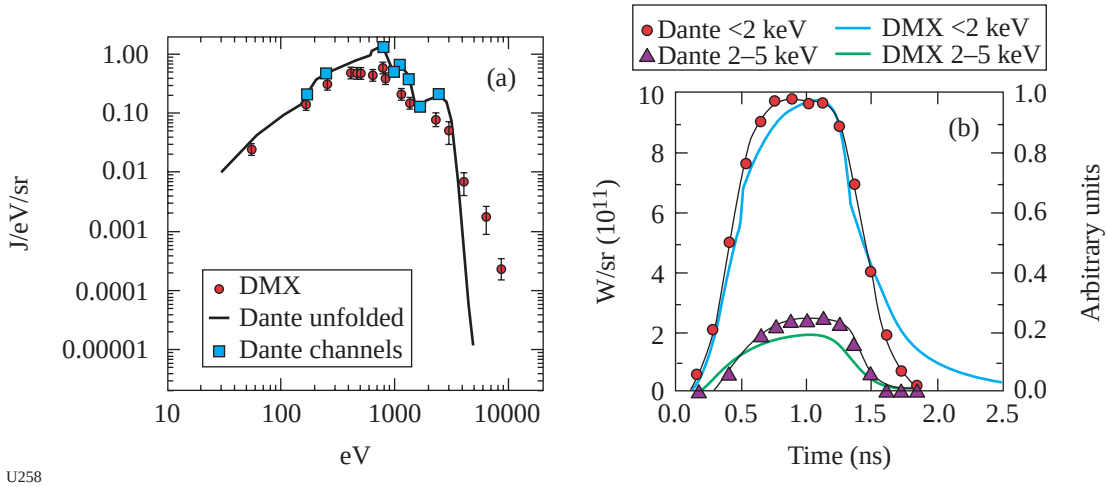

Figure 84.64
DMX/Dante experimental results comparison. (a) Time-integrated spectrum inferred from Dante (solid line and squares) and DMX (circles) on OMEGA Shot 18326. Symbols denote the mean energies of the channels for both diagnostics. (b) Spectrally integrated intensity as a function of time for $h\nu < 2$ keV and $2 < h\nu < 5$ keV. DMX data were rescaled with the same factor for both plots.

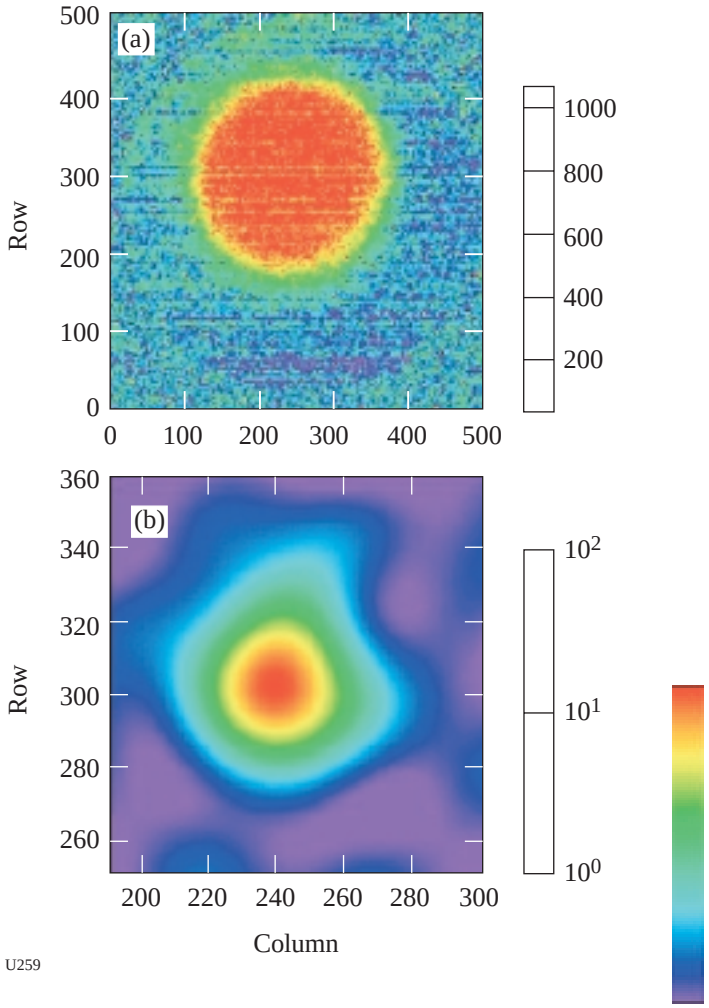

Figure 84.65
(a) Penumbral image of an imploded DT target. The central disk is the image of the neutrons passing through the entrance of the aperture. The neutron source size information is in the area surrounding the central disk. (b) Processed neutron image of a DT imploded target (Shot 20290). Ten pixels represent 28 μm on this image.